Published in final edited form as:
Annu Rev Chem Biomol Eng. 2012 ; 3: 103–127. doi:10.1146/annurev-chembioeng-062011-080930.

Design of Nanomaterial Synthesis by Aerosol Processes

Beat Buesser and **Sotiris E. Pratsinis**
Particle Technology Laboratory, Institute of Process Engineering, Department of Mechanical and Process Engineering, ETH Zurich, CH-8092 Zurich, Switzerland

Abstract

Aerosol synthesis of materials is a vibrant field of particle technology and chemical reaction engineering. Examples include the manufacture of carbon blacks, fumed SiO_2, pigmentary TiO_2, ZnO vulcanizing catalysts, filamentary Ni, and optical fibers, materials that impact transportation, construction, pharmaceuticals, energy, and communications. Parallel to this, development of novel, scalable aerosol processes has enabled synthesis of new functional nanomaterials (e.g., catalysts, biomaterials, electroceramics) and devices (e.g., gas sensors). This review provides an access point for engineers to the multiscale design of aerosol reactors for the synthesis of nanomaterials using continuum, mesoscale, molecular dynamics, and quantum mechanics models spanning 10 and 15 orders of magnitude in length and time, respectively. Key design features are the rapid chemistry; the high particle concentrations but low volume fractions; the attainment of a self-preserving particle size distribution by coagulation; the ratio of the characteristic times of coagulation and sintering, which controls the extent of particle aggregation; and the narrowing of the aggregate primary particle size distribution by sintering.

Keywords

aggregate particles; agglomerate particles; coagulation; coalescence; sintering; functional nanoparticles; multiscale modeling; flame aerosol reactors

INTRODUCTION

Everyday **aerosols** are seen as clouds, fog, smoke, or sprays. Less obviously, 28 wt% of each tire consists of fluffy, aerosol-made carbon black particles. If not for these particles, whenever one changed the oil in a car, one would have to change the tires as well. Even though still we do not know for sure how such particles increase the strength of rubber, we certainly take advantage of it.

Aerosol-made materials and aerosol processes are almost everywhere (1). For example, in drug tablets, fumed silica serves as an excipient material. Aerosols are found in cosmetics from powdered makeup to hair sprays as well as in lightguides for telecommunications. ZnO is a vulcanizing agent in the curing of rubber, and filamentary nickel is a key component in battery electrodes (1a). More than 60% of the worldwide production of white titania pigments, which are in every paint as an opacifier, is made by flame aerosol technology via the so-called chloride process. Nearly every gas- or diesel-powered motor vehicle is

buesser@ptl.mavt.ethz.ch, pratsinis@ptl.mavt.ethz.ch.

DISCLOSURE STATEMENT
The authors are not aware of any affiliations, memberships, funding, or financial holdings that might be perceived as affecting the objectivity of this review.

Europe PMC Funders Author Manuscripts

equipped with efficient fuel injection and downstream filters to capture the diesel soot in the exhaust. Furthermore, the UNIPOL process uses aerosols for the gas-phase manufacture of polyethylene and other polymers. Today aerosol processes are used worldwide with production rates up to several tons per hour to create multibillion U.S. dollar businesses (2).

The broad use of aerosol processes stems from their distinct advantages over wet and solid-phase chemistry processes (3): (*a*) no liquid by-products; (*b*) easier and cheaper particle collection; (*c*) fewer process steps; (*d*) transport phenomena (e.g., diffusion) in gases afford more rigorous treatment, which facilitates process design that leads to products of (*e*) high purity (e.g., optical fibers), (*f*) unique filamentary morphology, and (*g*) nonequilibrium metastable phases (4). To benefit from these advantages, one must also deal with some disadvantages (5): (*a*) high temperatures can lead to **aggregates** (hard **agglomerates**) that are not breakable into their constituent **(primary) particles (PPs)**; (*b*) low-cost precursors for economical manufacturing can lead to product contamination or may not even be available; (*c*) hollow, porous or inhomogeneous particle morphologies can occur; (*d*) the particle size distribution is usually polydisperse; and (*e*) particle growth is much faster than in liquids, which requires clever design for process scale-up. Control of these advantages and disadvantages is the art of engineering in the aerosol synthesis of materials.

The historic development of industrial aerosol processes for the synthesis of commodities has been summarized recently along with the new sophisticated materials and even devices made by such processes (6). Among them, flame spray pyrolysis (7, 8) and plasmas (9, 10) are most promising for efficient synthesis of an array of nanomaterials and even devices (4).

More specific to aerosol process design, Kraft (11) has reviewed elegantly the basic aerosol phenomena during flame synthesis of nanomaterials, highlighting sectional, moment, and Monte Carlo particle methods for simulating particle dynamics in laminar and turbulent flows. In a fascinating survey of nearly 600 articles, Barnard (12) pointed out the merits of various computational techniques in describing **nanoparticle** formation, structure, and phase transformations. Catlow et al. (13) have reviewed simulated **nanocluster** structures and their promising properties, which await experimental confirmation.

This review envisions (chemical) engineers confronted with the design of aerosol processes for nanomaterial synthesis: a daunting task given the limited knowledge of product properties and a priori process understanding. First, the process sequence is introduced with a focus on its critical components (reaction and heat transfer). Then key characteristics of nanomaterials are identified with a focus on the unique filamentary structure of aggregates and agglomerates consisting of PPs. The dominant aerosol phenomena (**coagulation** and sintering) that are responsible for this structure are highlighted along with the unique features that facilitate multiscale aerosol process design for nanomaterial synthesis.

Classic continuum models (Figure 1*a,b*) describe the effect of process variables (e.g., temperature, concentration) on product characteristics (e.g., particle size, morphology, crystallinity) over the entire process residence time and reactor volume. Depending on the state of knowledge about the nanoparticle properties (e.g., diffusivity, coagulation, or sintering rate), models with increasing sophistication are employed for property determination. For example, mesoscale models that treat particles as geometric bodies are used to calculate the **coalescence** rate (Figure 1*c*) or the transport properties and coagulation rate (Figure 1*d*) of multiparticle structures that are not adequately described by single spheres in conventional continuum models. More accurately and elegantly, the two-particle coalescence rate (Figure 1*e*) of such structures can be described by **molecular dynamics** models accounting for the interatomic interactions with pairwise potentials. These potentials

can be determined with quantum mechanics models that account for the electronic structure of matter.

The multiscale modeling is elucidated with particle dynamics and chemistry along with the fluid mechanics that frame process design for aerosol synthesis of materials. Finally, the unique features of aerosols in process design are summarized to highlight some of their emerging applications.

PROCESS OVERVIEW

Figure 2 shows the steps in the **aerosol** synthesis of nanomaterials from raw materials to reactor and cooling sections to eventual particle collection with gas treatment and recycling. Coating and functionalization are shown as side pathways, as they are carried out typically by wet chemistry processes. There is keen interest in bringing them to the gas phase to facilitate aerosol synthesis of the final products in one sequence.

Raw Materials

Depending on intended product composition, appropriate precursors are selected and aerosolized to facilitate their rapid conversion to the final product. Economics dictate the lowest possible precursor cost, although high-end products (e.g., biomaterials) can afford far costlier raw materials. Gaseous precursors are preferred but are rarely available; a notable example is gaseous SiH_4, which is used in the synthesis of silicon metal, originally for microelectronics (14) and recently for solar applications (15). Typically, liquids such as $Ni(CO)_4$, $TiCl_4$, or $SiCl_4$ and more rarely solids such as metals (used in inert gas condensation) (16) or halides (e.g., $AlCl_3$) are evaporated/sublimated and then thermally decompose or react with O_2 or air for the commercial synthesis of metal and ceramic particles.

Liquid precursors can be sprayed directly into the reactor to undergo evaporation and (partial) combustion, as occurs for hydrocarbons in the manufacture of carbon blacks (17). More recently, precursor solutions have been sprayed and combusted for the synthesis of an array of sophisticated mixed ceramics (18) and metals (19) by judicious selection of precursor and solvent composition (20). Even solid precursors can be dispersed in hot-wall (21), plasma (22), and flame reactors (23), although dosing of solids to maintain constant product composition is more challenging than that of gases or liquids.

Reactors

The reactor provides the high-energy environment needed to evaporate the precursor and/or drive the chemical reactions in material synthesis. Various types of reactors have been developed. A flame reactor is the simplest and energetically most favorable (24) because the energy of the precursors and fuels is used directly for synthesis of powders and films. As a result, flame reactors produce 80--90% by value and volume of the commercially available aerosol-made products today (2) and are most promising for the synthesis of catalysts (25), metals and biomaterials (19), gas sensors (26), magnetic nanocomposites (27), and even nutritional materials (28).

Hot-wall reactors use fuel combustion or electricity to heat precursors as they flow through a ceramic or metal tube in order to evaporate solids (e.g., Zn metal for synthesis of ZnO catalysts for rubber vulcanization), to drive $SiCl_4$ oxidation in lightguide preform fabrication, to decompose SiH_4 for silicon synthesis (14), to decompose $Ni(CO)_4$ for synthesis of filamentary Ni (29), and to pyrolyze sprays of inorganic salt solutions (30) or powder mixtures by laser flash evaporation (31) for the synthesis of carbides, borides, and other materials (21). Hot-wall reactors have well-defined temperature and residence time

distributions and produce approximately 10% by volume and value of commercially available aerosol-made products (2).

Plasma reactors use various electrode configurations to create a gas containing electrons, ions, and/or charged **nanoparticles** (plasma) (9). Plasma reactors can produce narrow particle size distributions (32, 33) because Coulomb forces limit Brownian **coagulation** (34). Extremely high temperatures (thermal plasmas) are capable of evaporation or decomposition of solid precursors (22). Low temperatures (nonequilibrium plasmas) are also possible for coating sensitive materials (35). Plasmas are used commercially to coat surfaces with ceramic and metal films (e.g., Nova AG) and are quite promising for chemical vapor deposition (CVD) synthesis of super-hard carbide films (36), luminescent Si nanoparticles (32, 33), and heterogeneous catalysts (10). Plasmas can be also created in other aerosol reactors when an electric field is generated, such as by placing needle or flat electrodes around the plume of an aerosol reactor (37) or by spark aerosol generators.

Microwave (38) and laser reactors (39) use a microwave cavity and a laser beam, respectively, to provide a high-energy environment and create a plasma as above (9). In addition, lasers are directed onto surfaces to get materials into the gas phase for the synthesis of nanomaterials by laser ablation (40). Microwave reactors have been used to make size-controlled Si nanoparticles on the laboratory scale at up to 10 g h^{-1} (41). Laser reactors have been considered for the synthesis of nonoxide materials and solar silicon, and start-up companies have even been created (e.g., Nanogram), but actual products have made little impact so far.

Inert gas condensation sparked the field of nanotechnology with the synthesis of nanostructured metals and ceramics (16, 42). This technique involves evaporation of metal vapor in low pressure, cooling by natural or forced convection, and collection of nanomaterials on cold surfaces. Although some start-up companies (e.g., Nanophase) have used inert gas condensation, few products have been made commercially, in contrast to the technique's academic impact.

Cooling

Typically, aerosols must be cooled properly for development of the desired crystallinity as well as for collection and storage. Drastic cooling can occur through direct spraying of water onto, for example, a freshly made carbon black plume to stop further combustion (17). However, cooling is done usually either by classic shell and tube heat exchangers (e.g., in the synthesis of rutile pigments) or by expansion of the freshly made aerosol plume (21). Aerosol reactors can provide extremely high cooling rates that permit capture of metastable crystal phases (25). Particle deposition to the cold tube walls must be avoided by all means. Significant effort has been devoted to this in large-scale manufacture of nanomaterials, as such deposits clog the process, and their resuspension contaminates the product (6).

Collection, Storage, and Gas Treatment

Particles are collected quite efficiently with cyclones and baghouse filters and stored in hoppers (17) or electrostatic precipitators (43). Filtration is reasonably well understood, although there is a continuous quest for lower costs, improved efficiency, and better understanding, especially of collection of ramified nanoparticles that form porous cake structures (44). Such structures possess high surface areas that can be easily contaminated, and contaminants can even induce changes in size and composition upon collection (45) and storage. The environment and temperature of collection and storage units is controlled to avoid undesired phase transformations, aggregation, and even dust explosions when combustible materials (e.g., carbon blacks, metal powders) are stored. In addition, the

hydration and fluffiness of particles must be preserved. Furthermore, prior to storage, process gases adsorbed on the particles [e.g., HCl on fumed silica (46) or H_2O on lightguide preforms (47)] are removed.

Direct aerosol deposition or collection by thermophoresis and/or impaction is used in the manufacture of lightguide preforms (47), refractory coatings (36), and Au electrodes for gas sensors (48, 49). Electrical fields are also used in deposition of ultrathin lines of nanoparticles for microelectronics (50). Gases accompanying the aerosol synthesis of materials are either recycled, as with the Cl_2 from titania production by oxidation of $TiCl_4$ used in chlorination of rutile and ilmenite ores, or sold separately, as with HCl in the synthesis of fumed silica and lightguide preforms by hydrolysis of $SiCl_4$. Another advantage of these chlorine cycles is that they do not produce CO_2 during their chemical reactions, in contrast to hydrocarbon-fed flames. In some processes, recyclable materials include solid by-products, for example, $TaCl_5$ reacting with Na vapors results in NaCl coatings during flame synthesis of tantalum powders with ultra-high surface area for electronics (51).

Conditioning: Coating and Functionalization

Rarely are particles used as prepared. Typically their functionality (opacity, magnetism, color) needs to be preserved while the particles are incorporated in appropriate liquid or solid matrices and devices. Coated particles can be formed in one aerosol step when the core and shell materials have vastly different precipitation rates and compatible surface energies, such as with V_2O_5-coated TiO_2 catalysts (52) or carbon-coated TiO_2 (53), $LiFePO_4$, (54) and metals (19).

Most commonly, however, coating and functionalization are carried out in liquid solutions. Particle surfaces are conditioned by precipitation or impregnation of thin layers or functional groups. This is followed by collection, drying, and mild annealing to avoid changes in core particle composition and morphology. This multistep task (55) essentially doubles the manufacturing cost of such particles (e.g., pigmentary titania).

As a result, there is interest in developing gas-phase coating and functionalization processes that can occur before particle collection (Figure 2). Freshly aerosol-made TiO_2, Fe_2O_3, Si, and Ag particles have been coated in situ with nanothin SiO_2 (56) or ZrO_2 shells (57) in sequential aerosol processes. The hermetic and smooth or granular texture of such shells is important for their applications (55). Lower process yield, however, because of the presence of unattached shell material or uncoated (bare) core particles, has motivated the development of continuum models for aerosol coating (58). In situ functionalization (attachment of organic groups) on such particles further facilitates their incorporation into liquidsand subsequent suspension stability (59). Atomic layer deposition has been used in fluidized beds to scalably coat particles with thin oxide layers (60). Molecular layer deposition followed by calcination has resulted in controlled pore diameter, high--surface area nanothin ceramic films (61).

PROCESS YIELD AND PARTICLE CHARACTERISTICS

Process Yield or Efficiency

The yield or simply the mass balance is the first condition to be satisfied in design simulations and benchmarking with experimental data. This is essential, as the finest particles can be lost easily during collection either by diffusion to reactor walls or escape with exhaust gases, which can distort comparisons between model predictions and data (see sidebar, Nanoparticle and Health). It is not unusual in laboratory units to have yields ranging from 50 to 90% depending on a single process variable, e.g., oxidant flow rate (62).

Typically, maximum yield is sought, which requires reactants to fully convert to the product. Aside from the obvious economics, process/product quality issues exist also. Particle deposits and accumulation to reactor walls can disrupt the process (reactor clogging) or deteriorate product quality by resuspension and inclusion in the product. Furthermore, partially converted precursors may deposit and contaminate the product particles. In some products, however, reduced yield can be tolerated to assure the high quality of the product, as is true for electronic films produced with CVD. For example, in the **aerosol** deposition of films, particles may escape target substrates to reduce substantially and acceptably the process yield. This also occurs in the synthesis of optical fiber preforms, which have particle deposition yields by thermophoresis of approximately 50% (63).

Morphology: Primary Particles, Aggregates, and Agglomerates

One of the key (and sometimes attractive) characteristics of aerosol-made materials is their filamentary structure. Aerosol processes form clusters of particles that are loosely attached to each other by physical forces (e.g., electrostatic, van der Waals) without any necking between the so-called **PPs**. These clusters are called soft agglomerates or just **agglomerates** and can be dispersed or broken into their constituent particles by applying adequate energy (e.g., shear, ultrasonic) (64). When PPs form necks between them, they are held together by chemical (e.g., covalent, ionic) forces. These are hard agglomerates or **aggregates** that are difficult to break into their constituent particles (65).

Agglomerates can be easily dispersed into liquid matrices, an attractive feature for paints and nanocomposites. Aggregates are preferred in catalyst pellets, lightguide preforms, and sensor films because they facilitate fluid transport between particles without restructuring that would collapse them into compact structures with smaller pores, which would result in high pressure drops and lower transport rates (64). Aggregates are particularly attractive for sensors and electroceramics because their necks form long crystal planes that minimize contact resistance as well as facilitate electron flow (66) and strong sensor signals (67).

The structure of aerosol-made agglomerates is similar to that of mathematical **fractals**, which greatly facilitates their description and processing. **Fractal-like** agglomerates (68) follow a power law relating their number of PPs, n_p, to agglomerate size (radius of gyration, r_g; mobility diameter, d_m; or projected area, a_a):

$$n_p = k_n \left(\frac{r_g}{r_p}\right)^{D_f} = k_m \left(\frac{d_m}{d_p}\right)^{D_{fm}} = k_a \left(\frac{a_a}{a_p}\right)^{D_a}, \quad 1.$$

where D_f, D_{fm}, and D_a are appropriate fractal dimensions; k_n, k_m, and k_a are appropriate preexponential factors (e.g., lacunarity); and r_p, d_p, and a_p are the PP radius, diameter, and surface area.

Aerosol-made agglomerates grow typically by diffusion-limited or ballistic cluster-cluster agglomeration (equivalent to **coagulation)** in the continuum or free-molecule regimes, respectively, with $D_f = 1.78$ (69) or 1.89 (70) and $k = 1.4 \pm 0.12$ or 1.36 ± 0.10, respectively (71). For sintered aggregates, D_f typically increases (72) all the way to $D_f = 3$ at full coalescence (73). Again, agglomerates made by collision of such aggregates would have $D_f = 1.8$--1.9. Agglomerates of polydisperse PPs and/or aggregates have smaller D_f values as their polydispersity increases (71). Recent mesoscale simulations indicate that during **coalescence** or sintering of such structures, a strong relationship exists between constituent PP number and diameter regardless of sintering mechanism and material composition (73a). Such relationships further facilitate characterization of these particles and greatly simplify process design.

Size

The size of PPs is essential for nanomaterial performance, whereas the size of their aggregates or agglomerates affects handling and processing. Both can be measured by counting particles in microscopic images, which requires at least 100 particles for a reliable average size and approximately 500 for polydispersity, e.g., geometric standard deviation (74). Nitrogen adsorption is used routinely to measure specific surface area and to determine the average PP size. By inversion of aerosol light scattering, the agglomerate or aggregate size lumped together (without distinction) can be obtained with some assumptions about the shape of their distribution, although the average PP size must be known, typically from microscopy (75). Small-angle X-ray or neutron scattering can be used to estimate all three sizes, as such wavelengths facilitate scanning four to five orders of particle sizes. Inversion of such spectra is not trivial, however, as it requires sophisticated software and assumptions about the shape of the size distributions. Nevertheless, it is possible to obtain quite reliable PP sizes and, most importantly, to distinguish between aggregate and agglomerate sizes (76), especially when such particles are dispersed in polymers (77).

Mass-mobility measurements offer the potential to measure the mobility and structure of aggregate or agglomerate particles without any assumptions about their size distribution shape (78). The degree of aggregation or agglomeration can be estimated by comparing the mobility and PP diameters (79).

Particle size measurements must be kept in mind when one designs aerosol processes and compares simulations with experimental data. For example, if diameters are compared, consistent averages of the particle size distribution should be used. For example, microscopy typically gives a number-average diameter, whereas nitrogen adsorption gives the Sauter diameter (a surface-volume average). Number-, surface-, and volume averages of the number or mass distribution of the same particle sample can differ by as much as 300% (80).

Crystallinity

The crystallinity of **nanoparticles** is often a key element in their performance. For example, rutile is preferred over anatase in pigmentary TiO_2 for its superior light scattering and opacity, whereas anatase is preferred in catalysis. Crystallinity is typically measured by X-ray diffraction with appropriate software to extract the crystal size and phase composition as well as the bimodal size distributions of a crystal phase. Comparable PP and crystal sizes indicate monocrystalline particles. Crystal phase composition is determined by the conditions in the reactor and cooling sections. For example, wustite, maghemite, or magnetite Fe_2O_3 can be made by flame spray pyrolysis by controlling the precursor and (oxidative or reducing) gas compositions (81). Dopants are also used to promote formation of specific phase compositions. For example, Al promotes synthesis of rutile, whereas Si promotes anatase TiO_2 (82) in hot-wall (79) and vapor- (37) and liquid-fed flame reactors (56).

DESIGN

Each process step (Figure 2) affects product particle characteristics. Therefore, a thorough design must account for all steps. However, two steps, reactor and cooling, determine crystal and grain or **PP** size and composition in a way that is nearly impossible to alter in subsequent processing or finishing (as it is called in practice). Thus, the design of reactor and cooling units is essential to the aerosol synthesis of materials. In the reactor, process temperature and pressure rapidly increase by either internal (flame) or external (hot-wall, laser beam, discharge) heating that drives precursor conversion as well as product aerosol formation and early growth. Once the precursors are consumed, the temperature gradually

drops, but aerosols continue to grow by coagulation and sintering, which results in the signature morphology of filamentary aerosol-made materials.

Figure 3 shows a typical evolution of average particle diameter by coagulation and sintering at nonisothermal conditions on a single streamline in an aerosol reactor (64). Early on (Figure 3 at $t < 8 \times 10^{-5}$ s), when the precursor has just been consumed and high temperature and small particle sizes prevail, the characteristic time for coagulation, τ_c, is much larger than that for sintering, τ_s. The PPs rapidly fuse upon collision, which results in compact particles until they reach a size (and/or temperature) at which $\tau_c \sim \tau_s$ (Figure 3 at $t \sim 8 \times 10^{-5}$ s). Then the coagulation and **coalescence** or sintering rates are comparable, which results in sinter bonds between colliding particles (onset of aggregation at d_{pN}). **Aggregates** of PPs are formed with diameter d_p. These aggregates have a characteristic size given by their collision diameter d_c. Later ($t \sim 4 \times 10^{-3}$ s), as the process temperature drops further, sintering practically stops ($\tau_s \rightarrow \infty$), and d_p and d_{cH} no longer change such that $\tau_c << \tau_s$ (onset of agglomeration). Sinter necks are no longer formed between colliding particles, which results in **agglomerates** of aggregates and/or single PPs depending on the duration of the aggregation phase ($\tau_c \sim \tau_s$).

To design aerosol processes for nanomaterial syntheses, one needs to quantitatively describe the above particle dynamics at nonisothermal conditions with fluid mechanics as well as the precursor chemistry using multiscale models of increasing sophistication depending on the uncertainty of the particle properties and available supporting information. For example, the diffusivities and coagulation rates of spherical particles (1--1,000 nm) are well understood through the Stokes-Einstein and Fuchs equations, respectively (83). As a result, they can be readily implemented in continuum models of fluid and particle dynamics to calculate particle growth and deposition on reactor walls (Figure 1*a,b*). In contrast, the diffusivity of aggregates or agglomerates, accounting for their size and structure, can be determined by mesoscale models (Figure 1*c,d*) before the diffusivities are employed in these continuum models. The above models also describe properties of agglomerates such as their diffusivity as well as the PP coordination number for use in **MD** simulations of particle sintering; determination of the evolution of agglomerate **fractal** dimension during fragmentation, restructuring or sintering (84); and calculation of the coagulation rate at high particle concentration (85) as an input parameter to continuum models.

MD simulations provide a much more detailed description of PP dynamics by treating each atom or ion separately. The increasing number of interactions between atoms that must be calculated, however, limits MD to systems that are smaller in both length and time. For bottom-up nanoparticle growth, the rate of particle coalescence (sintering) is important. The nanoparticle sintering rate can be described by MD through the detailed atomic motion from interatomic potentials, but these are not available for every material and especially for material mixtures. Development of such potentials is not easy and is frequently based on empirical fits to macroscopic properties (e.g., crystal lattice, elasticity) or more conveniently on simplified results of quantum mechanics calculations based on first principles (86).

With MD it is possible to obtain the characteristic sintering times (Figure 1*e*) of nanoparticles (87) or evaporation rates (Figure 1*f*) of nanodroplets (88). Such information can be used, for example, in mesoscale and continuum models of aggregates undergoing sintering for use in continuum reactor design models. Furthermore, MD simulations with classic potentials accelerate the search for minimum energy structures for geometry optimization calculations with quantum mechanics methods (89), which allow accurate material simulations but are limited to tiny systems on the order of 10 to 100 atoms depending on accuracy. Quantum mechanics models allow investigation of chemical reaction rates and mechanisms that can be incorporated directly into continuum models.

Combination of these methods leads to multiscale models for aerosol processes that describe the effect of process variables (precursor concentration, flow rate, temperature, cooling rate) on product particle characteristics (primary, aggregate, and agglomerate size, size distribution, morphology, and structure) that determine performance (4) in passive nanostructures (coatings, dispersions) and active devices (sensors, battery cells, etc.). Particle dynamics, chemistry, and fluid mechanics constitute the established continuum models in the design of aerosol processes in material synthesis, as examined below.

Particle Dynamics

Despite the high particle concentrations used in the **aerosol** synthesis of materials even at industrial conditions (e.g., titania production), rather small ($\phi = 10^{-3}$--10^{-4}) solid volume fractions are employed at huge Re numbers, up to 10^5--10^6, and production rates up to 25 t h^{-1}. Following Levenspiel's classification, these reactors are best characterized as transport reactors (3). In contrast to packed ($\varphi = 0.5$) or fluidized beds ($\varphi = 0.01$--0.1) in which particles affect fluid flow, in aerosol reactors particles barely influence fluid flow, chemistry, and process temperature. As a result, analytical (e.g., laminar flow) or numerical solutions [via computational fluid dynamics (CFD)] to momentum, energy, and mass balances (Navier-Stokes equations) give the temperature and velocity profiles of reactive flows (90). Then the evolution of particle characteristics along the reactor can be described by the general dynamics equation for aerosols for the rate of change of particle concentration, $n(v_p, t)$, of volume, v_p (68):

$$\frac{\partial n\left(v_p,t\right)}{\partial t}=\int_{v_m}^{v_p}\beta\left(v_p-v,v\right)n\left(v_p-v,t\right)dv-\frac{1}{2}n\left(v_p,t\right)\int_{v_p}^{\infty}\beta\left(v_p,v\right)n\left(v,t\right)dv$$
$$+S\left(v_p,t\right)\delta\left(v_p-v_m\right)+\frac{\partial}{\partial v_p}\left(I\left(v_p,t\right)n\left(v_p,t\right)\right) \quad 2.$$

The first two right-hand-side terms account for **coagulation**, the third for nucleation, and the last for condensation or surface growth. Depending on how particle shape is quantified (length, surface, volume, structure), this equation must be written in two or more particle variables (or size dimensions). For the typical **fractal-like particles** made by aerosol processes (see section on morphology and structure above), Equation 2 is solved using volume and surface area as the two particle size dimensions by extending a 1D sectional technique (91) to the two size dimensions (92). That way the interplay of coagulation and coalescence is elucidated through the evolution of the detailed particle volume and surface area distributions, which provides process insight. This explains, for example, why fumed silica has a more filamentary structure than titania made at identical hot-wall reactor conditions, in accord with experimental data (93). This knowledge also facilitates the development of simpler models (94) that capture the essence of the process and can be readily interfaced with chemistry and fluid dynamics models, as shown below. Despite their computational demands, even 3D (finite volume) population balances are now routinely used throughout particle technology (e.g., granulation) with particle size, binder content, and agglomerate porosity as variables (95).

Nevertheless, the computational demands of detailed representations of the size distribution have motivated the development of models in terms of the moments of that distribution. Various approaches have been used to close these moments by forcing a lognormal shape (96, 97), interpolating between integer moments (98), or using more elaborate schemes (99) addressing even multidimensional size distributions (100, 101). A disadvantage of moment models is associated with the nonuniqueness of reconstruction of the particle size distribution from its moments (11, 98). Nevertheless, moment models have been used in the design and operation of lathes for fabrication of lightguide performs by modified CVD

(MCVD) on an industrial scale; in this case the focus was more on the particle deposition rate and efficiency rather than on the size distribution (102).

Simplified Particle Dynamics—There are, however, unique process features during the aerosol synthesis of materials that can simplify the quantitative description of particle dynamics, as summarized here:

1. Typically, precursors react quickly to yield high particle concentrations. As a result, Brownian coagulation dominates aerosol dynamics, rather than nucleation and condensation, which are dominant, for example, with atmospheric aerosols (83).

2. Such highly concentrated aerosols attain a **self-preserving size distribution (SPSD)** by coagulation (103) quickly, e.g., by the time they have grown to two to three times their initial size (104) or to the size (a few nanometers) at the end of chemical reaction (105). As a result, particles obtain a size distribution with a constant number-based geometric standard deviation (105), σ_g = 1.44--1.46, even though they continue to grow. Notably, in their legendary paper Granqvist & Buhrman (42) made **nanoparticles** of ten different metals by inert gas condensation, and all had σ_g = 1.48 ± 0.12. Therefore, coagulation dynamics can be followed by a single moment (e.g., the total number concentration, N):

$$\frac{dN}{dt} = -\frac{1}{2}\beta N^2, \quad 3.$$

where β is the collision frequency (83). From the N and a mass balance for the total particle mass or volume concentrations, V, the average particle diameter, d, is:

$$d = \left(\frac{6V}{\pi N}\right)^{\frac{1}{3}}. \quad 4.$$

From d and σ_g, the complete particle size distribution can be reconstructed at any process residence time.

3. When particles do not coalesce upon collision, fractal-like agglomerates (grape-like structures) of radius r_g are formed that consist of n_p **PP**s of radius r_p following a power law (Equation 1) with D_f = 1.8--1.9 (69, 70). This is attained when $n_p > 10$ (106). The collision frequency of agglomerates can be estimated from the above β for spheres (Equation 3) by replacing d with the agglomerate collision diameter, d_c:

$$d_c = \frac{6V}{A}\left(\frac{A^3}{36\pi V^2}\right)^{\frac{1}{D_f}}, \quad 5.$$

where A is the total surface area concentration of agglomerates. They also obtain a SPSD, which is slightly broader than that described above for spheres (107). There is a need, however, for more rigorous expressions for such β values that can be obtained from mesoscale models (Figure 1*c*).

4. When PPs within an agglomerate fuse or sinter, they become aggregates that are more compact than agglomerates (72, 75), and their surface area, a (= A/N), follows a phenomenological rate (108):

$$\frac{da}{dt} = -\frac{a - a_{fc}}{\tau_s}, \quad 6.$$

where τ_s is the characteristic time for sintering and depends on material composition, particle size, and temperature. This is the time needed for particles to reduce their excess surface area ($a - a_{fc}$) over that of a sphere of equal mass by 63% (92). Equation 6 has explained quantitatively the **coalescence** of nonspherical SiO_2, TiO_2, B_4C, Ag, and PdO (37) by adjusting the parameters of the corresponding τ_s to the material composition and/or process configuration (e.g., by lumping fluid mechanics and composition). More rigorous expressions are obtained for particle ensembles by mesoscale (109) and even MD models (87).

5. The PP size distribution within aggregates narrows as particles sinter in inverse proportion to their size (110), similar to aerosol condensation (83), as sintering rates are inversely proportional to particle diameter.

6. Turbulence barely affects PPs (111) but affects agglomerate particle size through enhanced coagulation (112), restructuring, and even fragmentation (104).

These features permit the use of unimodal aerosol dynamics models (113) accounting for reaction, coagulation, and sintering (94) as well as surface growth (74) and even the use of bimodal models (114) that can be readily interfaced with fluid dynamics. This approach works well for the synthesis of particles large enough that coagulation washes out any chemistry effects on product particle sizes. During particle formation, a nucleation and a coagulation mode are formed, and the average particle diameter substantially underpredicts measured particle sizes, as it averages the numerous product molecules (monomers) with molecular clusters or particles. Once particle formation ceases, however, the diameters are within 20% of those predicted by detailed models such as Equation 2 (74).

Chemistry

The chemistry of **aerosol** formation determines particle composition and crystallinity as well as the mass balance and production rate of the process. In particle manufacture, usually complete reactant conversion is sought, so every effort is made to achieve complete conversion without close attention to its intricate detail. As a result, overall reaction rates in terms of the limiting reactant (precursor) are used in the oxidation of $TiCl_4$ for production of titania (115) or $SiCl_4$ for production of lightguide performs by MCVD (116). These rates can be used to compare characteristic times for chemical reaction with those for turbulent mixing in schemes to estimate equipment-specific formation rates of product. In addition, they are used to determine the temperature and velocity profiles in the reactor and to monitor precursor conversion and avoid precursor breakthrough and condensation to product particles. These overall chemistry models are readily interfaced with fluid and particle dynamics in diffusion flame aerosol reactors for SiO_2 (117) and Cr_2O_3 (118), in premixed flames for TiO_2 (74), in hot wall reactors for SiO_2 (119) and TiO_2 (120), and for lightguide performs by MCVD. When such reaction rates are extremely fast, it is possible to treat the particle formation as reactant-mixing limited in detailed chemistry and fluid mechanics computational models (117).

In film synthesis (e.g., CVD of Si) only a fraction of the reactant (e.g., SiH_4) is converted because a key process goal is to prevent snow formation and particle deposition that would ruin the film uniformity. As a result, close attention is paid to the chemistry of silane decomposition (121), and detailed models have been developed to interface silane chemistry and fluid mechanics in various reactor configurations (122, 123). Recently, more detailed

chemistry models have been developed for $SiCl_4$ hydrolysis in the absence of particles (124) and for $TiCl_4$ oxidation (125).

In most of these processes, gas-phase kinetics dominate precursor conversion. In the synthesis of carbon black, however, most soot formation takes place via surface growth. Note, however, that approximately half of the precursor is oxidized to pyrolyze the other half to produce carbon black. Nevertheless, the energy released from hydrocarbon oxidation seems to be much larger than that generated by surface growth, as it dominates the reactor temperature-velocity profile and maintains the one-way coupling in simulations of such reactors (11, 126). In filamentary Ni or Fe metal synthesis by carbonyl decomposition, surface growth is dominant, but external heating by electric elements dominates the process temperature, and again the one-way coupling is preserved (29).

If the chemistry, however, dominates the process (autocatalysis) or highly ramified particles are formed that influence far more reactor volume than their solid volume fraction, detailed interfacing of particle and fluid dynamics might be needed, as is used in modeling transport phenomena in fluidized beds. This could be the case when high precursor volume fractions (e.g., 10 vol.% $SiCl_4$) lead to production of micrometer-sized **agglomerates** of fine (<10 nm) nanoparticles (127).

Fast chemical reactions are typical in the aerosol synthesis of materials. Naturally, they result in high concentrations of product molecules (monomers) and nanoclusters that grow immediately by coagulation, because their critical nucleation size at typical reactor conditions is smaller than that of a single monomer/molecule (111). But this macroscopic view of coagulation might not be the final answer to the initial growth of **nanoclusters** (13). From a detailed mechanism of $TiCl_4$ oxidation with 64 reactions, West et al. (125) found that the critical nucleation size of TiO_2 consists of five such molecules. Bromley & Illas (128) compared the total energy (relative stability) of $(SiO_2)_N$ nanoclusters and found that, although the overall trend indicates that larger N leads to more stable SiO_2 clusters, certain N are more stable than $N-1$ and $N+1$, thus creating a series of magic N that might represent the energetically most favorable cluster growth path. However, this effect diminished for bigger particles approaching continuum.

From a multiscale perspective, Hamad et al. (89) investigated the global energy minima of small $(TiO_2)_N$ nanoclusters for $N = 1$--15. They found that classical **MD** potentials for TiO_2, which can be used for simulations of particles of several nanometers, can describe $(TiO_2)_N$ in terms of energy and geometry in quite good agreement with the more expensive quantum mechanical density functional theory (DFT) method for $N > 9$.

Furthermore, there is keen interest in the early stages of particle formation, as chemistry determines the phase composition of the early clusters. Detailed chemistry computations are used to identify these clusters (13). But much needs to be done. For example, DFT computations have not yet revealed the rutile promotion effect obtained by doping TiO_2 formation with Al (129), which is observed experimentally (72) and widely practiced in the pigment industry (130). However, far more chemistry research into this early stage of particle formation is expected. In addition, the development of gas-phase coating or functionalization processes requires a quantitative understanding of the pertinent chemistry on par with that of CVD of films in order to achieve efficient and hermetic particle coatings of controlled smooth or rough texture (58).

Fluid Mechanics

As in all chemical reactors, CFD models give the all-important residence time distribution of particles, especially at high temperatures. This reveals classical pathological problems in the

reactor such as recirculation zones or dead volumes. As a result, readily available, commercial CFD software packages are used routinely in industry to design and operate aerosol reactors. They are used also in academia to trace the sources of extreme or unusual product particle characteristics and redesign experiments. For example, highly bimodal size distributions of Bi **nanoparticles** were traced to premature particle formation and recirculation in the evaporation zone of Bi metal vapor generation, which led to new mixing heads for the hot metal vapor and cooling gas (45).

Early combinations of CFD and particle dynamics addressed laminar flows. For example, such simulations showed that **coagulation** increases the size of newly formed silica so that Brownian diffusion no longer dominates particle deposition to lightguide preform walls; this makes thermophoresis the dominant transport mechanism in perform fabrication by MCVD (63). MCVD is one of the few industrial processes in which detailed aerosol process design was employed all the way down to the production lines. Also, Yu et al. (118) modeled chromium oxide formation by detailed aerosol dynamics in laminar diffusion flames in reasonable agreement with data in the free molecule regime. Bensberg et al. (131) showed that limited radial diffusion of freshly made Si_3N_4 particles in hot-wall laminar flows led to a broader size distribution than the **SPSD**.

Most investigations of turbulent reactors rely on Reynolds-averaged Navier Stokes (RANS) turbulence models, either standard k-ε, realizable k-ε (132), or Reynolds stress model (RSM) (133). The RSM is more demanding, as it adds six additional equations to the solution, whereas the k-ε models require only two. However, it often returns more accurate results, such as with swirling flows (134), whereas the realizable k-ε leads to better results than the standard k-ε and resolves the round-jet anomaly (132).

Turbulent diffusion flames producing Al_2O_3 and TiO_2 (135) nanoparticles have been simulated by **RSM** to extract an effective sintering rate of titania to reproduce a measured specific surface area at various flame conditions. Ji et al. (136) simulated nanoparticle synthesis in hydrogen flame reactors by implementing moments of the size distribution in CFD and accounting for particle growth by condensation and chemical reaction in agreement with measurements (137) when adjusting the particle formation and growth rates. Manenti & Masi (138) used CFD to design tangenti-based nozzles for flame aerosol reactors to reduce recirculation and broadening of the particle size distribution without distinguishing between primary and agglomerate particles. Widiyastuti et al. (23) included nucleation, coagulation, evaporation, and condensation in solid-fed flame synthesis of silica by CFD in agreement with field-emission scanning electron microscope measurements.

Direct numerical simulation (DNS) describes turbulence flows most accurately by accounting for all of their length and time scales. Therefore, the grid must be fine enough to resolve the smallest length scale of turbulence, the Kolmogorov scale η, and be large enough to describe the characteristic size of the simulated geometry. The extremely high computational demand of DNS confines it to local problems such as boundaries between different flows or simple jet configurations. Thus, coagulation of nanoparticles in 2D, incompressible, isothermal mixing layers of coflowing streams of different velocities has been investigated by DNS in combination with moment (lognormal) representation of the particle size distribution (139) to reveal concentration gradients inside the turbulence eddies.

Large eddy simulations (LESs) are less demanding than DNS but more demanding than **RANS** models because **LESs** resolve the large-scale motion of the turbulence exactly, but models are applied to the unresolved subgrid-scale turbulence. LESs of planar jets have shown that large eddies distort the homogeneous particle concentration fields, but eddies that merge together result again in more homogeneous fields (140). Recently, LES has been

combined with moment models (101) and detailed chemistry (125) to simulate (141, 142) titania formation in classic diffusion flames (143) without accounting for sintering.

Fluid and particle dynamics can guide quite effectively the design of novel aerosol processes, such as the in-situ coating of freshly made nanoparticles, when rather few experimental data are available. For example, the process variables (mixing of core aerosol with shell precursor vapor) that affect most effectively the hermetic coating of titania particles by nanothin silica films were identified (58), which facilitated efficient experimentation and screening of potential reactor configurations.

CONCLUDING REMARKS

There is no doubt that **aerosol** technology has contributed decisively to the development of many products and business sectors to create value and jobs. It is fascinating to see the creation of new aerosol products and scalable processes, especially in connection to nanotechnology and life sciences. Synthesis of a spectrum of heterogeneous catalysts by aerosol technology is rapidly gaining traction even in industrial settings (e.g., at Johnson-Matthey). Also, an array of biomaterials for dental prosthetics and bone replacements are under development and evaluation with animals. Spinoff companies are making functionalized cobalt- and iron-based magnetic nanoparticle suspensions that are broadly used in biosystems. Nanosilver made in flames is incorporated in polymer films and fibers for textiles to take advantage of its antibacterial and antiseptic properties. Furthermore, aerosol-made nanominerals (Fe, Zn, Ca, Mg) that can be readily dissolved in the low pH of the stomach are being evaluated as nutritional supplements (28). Patterned aerosol deposition of nanostructures (spots or lines) on select substrates creates the opportunity to build memory devices (144), Li battery electrodes (145), and highly selective gas sensors for acetone vapor in the human breath for monitoring diabetes (146).

For both established and budding applications, efficient process design is essential for industrial implementation of aerosol technology. This design is challenging because it involves solids processing that is far more complex than dealing with gases or liquids. The reactive turbulent flows and highly concentrated aerosols with filamentary or **fractal-like particle** structure pose the major hurdles. Unsurprisingly, most of the early process development for manufacture of carbon blacks, pigmentary titania, and fumed silica relied on evolutionary research and empiricism in the mid- to late twentieth century. In contrast, manufacture of optical fibers by thermophoretic aerosol deposition of successive layers of graded refractive index silica from laminar flows relied on solid chemical engineering in the mid-1980s. This shows clearly that when the science is accessible, industry will use it.

In the past 20 years, mostly academic research has addressed these challenges, making aerosol process design far more attractive by sound aerosol science and technology. Most notably, the high particle concentrations make coagulation the dominant aerosol phenomenon, in stark contrast to environmental aerosols for which nucleation, condensation, or surface growth dominate aerosol formation and transport. This assures a rapid attainment of the SPSD which in turn permits describing the particle size distribution by a single moment. That way aerosol particle dynamics are greatly simplified and efficiently incorporated into fluid mechanics simulations to elucidate aerosol processes in detail. In this way the effect of process variables on product aerosol characteristics can be unraveled for efficient process design and operation.

The dominance of coagulation also simplifies the description of chemistry during the aerosol synthesis of materials because coagulation is forgiving and forgetting uncertainties in early process stages. Although precursor chemistry plays a critical role in early formation of the

crystalline structure and/or composition, it tends to have little influence on the final product characteristics, as the chemistry tends to be completed rather quickly compared with particle growth. In addition, the formation of multicomponent particles with combined functionalities is quite challenging because the properties of mixed materials are difficult to determine a priori.

Furthermore, the extent of aggregation of the **fractal**-like structures is traced to the relative rates of particle coagulation and **coalescence**. Although the coalescence rate is not understood as well as the collision rate of spherical particles, phenomenological expressions (when available) allow for a quantitative description of the evolution of clusters of loosely attached particles (**agglomerates**) to hard- or sinter-necked ones (**aggregates**), to fully compact or fused ones (e.g., spheres), to many ceramic and metal particles. This is an area of active research, as the sintering rates of powder compacts can be used as a starting point for the coalescence rate of unconstrained particles in the gas phase. Clearly, distinct differences exist between packed particle beds undergoing coarsening in conventional sintering ovens and particle ensembles free flowing through an aerosol reactor.

The intimidating irregular structure of agglomerates can be characterized by power laws, which capitalizes on advancements in fractals. In particular, diffusion-limited and ballistic cluster-cluster agglomeration are quite similar to the coagulation of noncoalescing particles with a well-defined fractal dimension, $D_f = 1.8\text{--}1.9$, and preexponential factor, $k = 1.4$. High particle concentrations mean that Brownian coagulation is the dominant particle growth mechanism. This leads to particles with a size distribution with a well-defined shape, the SPSD. The formation of sinter-bonded aggregates facilitates the narrowing of the size distribution of their constituent **PP**s, similar to aerosol condensation, as the sintering rate is also inversely proportional to particle size. This enables aerosol-made materials to perform similarly to wet-made monodisperse particles; for example, absorption spectra shift with decreasing ZnO crystal size without any size segregation (147).

In summary, although a lot needs to be learned in this interface of physical chemistry, mathematics, and materials science, enough is known to make sophisticated nanomaterials on a large scale by aerosol processes using sound chemical reaction engineering and principles of aerosol particle technology. Plenty of design tools at various levels of complexity await to attract and challenge chemical and process engineers: Classic continuum, mesoscale, MD, and even quantum mechanics models address topics from industrial-level reactive processes down to the electronic state of molecules. The choice and application of such models depends on the end use of the product and the current state of knowledge of its properties.

Nanoparticles and Health

Nanoparticles are of great interest in life science systems and applications. On the one hand, nanoparticles are potentially hazardous in lungs and cells because of their size, shape, solubility, and concentration (148); on the other hand, they are promising as therapeutics (thermal cancer treatment), diagnostics (contrast agent for tomography), and curing agents (drug delivery). Laboratory and workplace safety requires continuous monitoring with appropriate devices to measure the particle concentrations governing the health risks (e.g., number, surface area, volume) (149). Furthermore, the health effects of engineered nanoparticles must be investigated with realistic particle morphologies and concentrations (150).

The established knowledge on nanoparticle growth and properties in aerosol processes provides the groundwork for understanding the fate of nanoparticles in biological and health-related systems. Existing multiscale models and simulations can provide insight into

nanoparticle transport properties in cells and across cell walls, solubility in cell plasma, shape, and morphology, all of which are directly related to their toxicity.

Acknowledgments

Financial support from Swiss National Science Foundation (SNF) Grant # 200021-119946/1 and the European Research Council is gratefully acknowledged.

TERMS AND DEFINITIONS LIST

Aerosol	suspension of solid or liquid particles in a gas; the particles are in continuous Brownian motion
Agglomerates	clusters of (primary) particles or spherules held together by weak physical (e.g., van der Waals, electrostatic, or capillary) forces
Aggregates	clusters of (primary) particles or spherules held together by strong chemical (e.g., sinter) forces; ridges or necks are formed between primary particles
Coagulation	the process by which two particles stick upon collision regardless of if they fuse together; also called flocculation, agglomeration, or granulation
Coalescence	the process by which two or more particles fuse into a single one; also called sintering
Fractal	non-euclidean geometric structure
Fractal-like particles	ensembles of clusters for which the number of constituent particles and gyration radius (or collision diameter or mobility diameter) follows a power law
LES	large eddy simulation
Molecular dynamics (MD)	simulations that describe the motion of single atoms with interatomic potentials
Nanocluster	a cluster of atoms with size smaller than ~1 nm, at which size properties begin to depend on the discrete number of atoms
Nanoparticle	particle with characteristic size between 1--100 nm, at which properties can start to differ from bulk ones considerably
Primary particle (PP)	basic particle for building larger fractal-like particles composed of one or several crystal grains. Their size determines properties such as opacity, superparamagnetism, and melting point
RANS	Reynolds-averaged Navier-Stokes
RSM	Reynolds stress model
Self-preserving size distribution (SPSD)	time-invariant shape size distribution of aerosols undergoing Brownian coagulation; dimensionless size distribution defined by its geometric standard deviation

LITERATURE CITED

1. Rosner DE. Combustion synthesis and materials processing. Chem. Eng. Edu. 1997; 31:228–35.

Europe PMC Funders Author Manuscripts

1a. Ulrich GD. Flame synthesis of fine particles. Chem. Eng. News. 1984; 62:22–29. [PubMed: 11541976] [Formulated the vision of flame aerosol technology for synthesis of a wide spectrum of materials.]

2. Wegner K, Pratsinis SE. Scale-up of nanoparticle synthesis in diffusion flame reactors. Chem. Eng. Sci. 2003; 58:4581–89.

3. Pratsinis SE, Mastrangelo SVR. Material synthesis in aerosol reactors. Chem. Eng. Prog. 1989; 85:62–66.

4. Pratsinis SE. Aerosol-based technologies in nanoscale manufacturing: from functional materials to devices through core chemical engineering. AIChE J. 2010; 56:3028–35.

5. Kodas, TT.; Hampden-Smith, MJ. Aerosol Processing of Materials. Wiley; New York: 1999.

6. Pratsinis, SE. History of manufacture of fine particles in high-temperature aerosol reactors. In: Ensor, D., editor. Manufacture of Fine Particles. RTI Press; Research Triangle Park, NC: 2011. p. 475-507. [Overview of the historic development of aerosol processes and latest applications.]

7. Bickmore CR, Waldner KF, Treadwell DR, Laine RM. Ultrafine spinel powders by flame spray pyrolysis of a magnesium aluminum double alkoxide. J. Am. Ceram. Soc. 1996; 79:1419–23.

8. Madler L, Kammler HK, Mueller R, Pratsinis SE. Controlled synthesis of nanostructured particles by flame spray pyrolysis. J. Aerosol Sci. 2002; 33:369–89.

9. Vollath D. Plasma synthesis of nanopowders. J. Nanopart. Res. 2008; 10:39–57. [A nice review focusing on highly promising plasma processes for particle synthesis.]

10. Phillips J, Luhrs CC, Richard M. Review: engineering particles using the aerosol-through-plasma method. IEEE Trans. Plasma Sci. 2009; 37:726–39.

11. Kraft M. Modelling of particulate processes. KONA. 2005; 23:18–35. [Detailed review of particle dynamics in modeling flame aerosol synthesis.]

12. Barnard AS. Modelling of nanoparticles: approaches to morphology and evolution. Rep. Prog. Phys. 2010; 73:086502.

13. Catlow CRA, Bromley ST, Hamad S, Mora-Fonz M, Sokol AA, Woodley SM. Modelling nano-clusters and nucleation. Phys. Chem. Chem. Phys. 2010; 12:786–811. [PubMed: 20066364]

14. Alam MK, Flagan RC. Controlled nucleation aerosol reactors: production of bulk silicon. Aerosol Sci. Technol. 1986; 5:237–48.

15. Knipping J, Wiggers H, Rellinghaus B, Roth P, Konjhodzic D, Meier C. Synthesis of high purity silicon nanoparticles in a low pressure microwave reactor. J. Nanosci. Nanotechnol. 2004; 4:1039–44. [PubMed: 15656199]

16. Gleiter H. Nanocrystalline materials. Prog. Mater. Sci. 1989; 33:223–315.

17. Kühner, G.; Voll, M.; Donnet, J-B.; Bansal, RC.; Wang, MJ.; Dekker, M. Carbon Black. CRC Press; New York: 1993. Manufacture of carbon black; p. 1-66.

18. Strobel R, Pratsinis SE. Flame aerosol synthesis of smart nanostructured materials. J. Mater. Chem. 2007; 17:4743–56. [Summary of the recent developments and discoveries of new and smart nanomaterials made in flames.]

19. Athanassiou EK, Grass RN, Stark WJ. Chemical aerosol engineering as a novel tool for material science: from oxides to salt and metal nanoparticles. Aerosol Sci. Technol. 2010; 44:161–72.

20. Teoh WY, Amal R, Madler L. Flame spray pyrolysis: an enabling technology for nanoparticles design and fabrication. Nanoscale. 2010; 2:1324–47. [PubMed: 20820719]

21. Weimer AW, Roach RP, Haney CN, Moore WG, Rafaniello W. Rapid carbothermal reduction of boron oxide in a graphite transport reactor. AIChE J. 1991; 37:759–68.

22. Ryu T, Choi YJ, Hwang S, Sohn HY, Kim I. Synthesis of yttria-stabilized zirconia nanopowders by a thermal plasma process. J. Am. Ceram. Soc. 2010; 93:3130–35.

23. Widiyastuti W, Purwanto A, Wang W-N, Iskandar F, Setyawan H, Okuyama K. Nanoparticle formation through solid-fed flame synthesis: experiment and modeling. AIChE J. 2009; 55:885–95.

24. Osterwalder N, Capello C, Hungerbühler K, Stark W. Energy consumption during nanoparticle production: How economic is dry synthesis? J. Nanopart. Res. 2006; 8:1–9.

25. Schimmoeller B, Pratsinis SE, Baiker A. Flame aerosol synthesis of metal oxide catalysts with unprecedented structural and catalytic properties. ChemCatChem. 2011; 3:1234–56.

26. Tricoli A, Righettoni M, Teleki A. Semiconductor gas sensors: dry synthesis and application. Angew. Chem. Int. Ed. 2010; 49:7632–59.
27. Wiggers H. Novel material properties based on flame-synthesized nanomaterials. KONA. 2009; 27:186–94.
28. Zimmermann MB, Hilty FM. Nanocompounds of iron and zinc: their potential in nutrition. Nanoscale. 2011; 3:2390–98. [PubMed: 21483965]
29. Wasmund EB, Saberi S, Coley KS. Modeling of an aerosol reactor for optimizing product properties. AIChE J. 2007; 53:1429–40.
30. Messing GL, Zhang SC, Jayanthi GV. Ceramic powder synthesis by spray pyrolysis. J. Am. Ceram. Soc. 1993; 76:2707–26.
31. Djenadic R, Akgül G, Attenkofer K, Winterer M. Chemical vapor synthesis and structural characterization of nanocrystalline $Zn_{1-x}Co_xO$ (x = 0-0.50) particles by X-ray diffraction and X-ray absorption spectroscopy. J. Phys. Chem. C. 2010; 114:9207–15.
32. Sankaran RM, Holunga D, Flagan RC, Giapis KP. Synthesis of blue luminescent Si nanoparticles using atmospheric-pressure microdischarges. Nano Lett. 2005; 5:537–41. [PubMed: 15755110]
33. Mangolini L, Thimsen E, Kortshagen U. High-yield plasma synthesis of luminescent silicon nanocrystals. Nano Lett. 2005; 5:655–59. [PubMed: 15826104]
34. Xiong Y, Pratsinis SE, Mastrangelo SVR. The effect of ionic additives on aerosol coagulation. J. Colloid Interf. Sci. 1992; 153:106–17.
35. Roth C, Künsch Z, Sonnenfeld A, Rudolf von Rohr P. Plasma surface modification of powders for pharmaceutical applications. Surf. Coat. Technol. 2011; 205(Suppl. 2):S597–600.
36. Liao F, Girshick SL, Mook WM, Gerberich WW, Zachariah MR. Superhard nanocrystalline silicon carbide films. Appl. Phys. Lett. 2005; 86:171913.
37. Pratsinis SE. Flame aerosol synthesis of ceramic powders. Prog. Energy Combust. Sci. 1998; 24:197–219.
38. Vollath D, Szabó DV. Synthesis of nanocrystalline MoS_2 and WS_2 in a microwave plasma. Mater. Lett. 1998; 35:236–44.
39. van Erven J, Munao D, Fu Z, Trzeciak TM, Janssen R, et al. The improvement and upscaling of a laser chemical vapor pyrolysis reactor. KONA. 2009; 27:157–73.
40. Semaltianos NG. Nanoparticles by laser ablation. Crit. Rev. Solid State Mater. Sci. 2010; 35:105–24.
41. Gupta A, Swihart MT, Wiggers H. Luminescent colloidal dispersion of silicon quantum dots from microwave plasma synthesis: exploring the photoluminescence behavior across the visible spectrum. Adv. Funct. Mater. 2009; 19:696–703.
42. Granqvist C, Buhrman R. Ultrafine metal particles. J. Appl. Phys. 1976; 47:2200–19.
43. Haas V, Birringer R, Gleiter H, Pratsinis SE. Synthesis of nanostructured powders in an aerosol flow condenser. J. Aerosol Sci. 1997; 28:1443–53. [A classic paper on the early development of processes for the synthesis of nanomaterials.]
44. Elmøe TD, Tricoli A, Grunwaldt J-D, Pratsinis SE. Filtration of nanoparticles: evolution of cake structure and pressure-drop. J. Aerosol Sci. 2009; 40:965–81.
45. Wegner K, Walker B, Tsantilis S, Pratsinis SE. Design of metal nanoparticle synthesis by vapor flow condensation. Chem. Eng. Sci. 2002; 57:1753–62.
46. Flesch J, Kerner D, Riemenschneider H, Reimert R. Experiments and modeling on the deacidification of agglomerates of nanoparticles in a fluidized bed. Powder Technol. 2008; 183:467–79.
47. Rowell JM. Photonic materials. Sci. Am. 1986; 255:146–57.
48. Madler L, Roessler A, Pratsinis SE, Sahm T, Gurlo A, et al. Direct formation of highly porous gas-sensing films by in situ thermophoretic deposition of flame-made Pt/SnO_2 nanoparticles. Sens. Actuators B. 2006; 114:283–95.
49. Liu Y, Koep E, Liu M. A highly sensitive and fast-responding SnO_2 sensor fabricated by combustion chemical vapor deposition. Chem. Mater. 2005; 17:3997–4000.
50. Krinke T, Fissan H, Deppert K, Magnusson M, Samuelson L. Positioning of nanometer-sized particles on flat surfaces by direct deposition from the gas phase. Appl. Phys. Lett. 2001; 78:3708.

51. Barr J, Axelbaum R, Macias M. Processing salt-encapsulated tantalum nanoparticles for high purity, ultra high surface area applications. J. Nanopart. Res. 2006; 8:11–22.
52. Stark WJ, Wegner K, Pratsinis SE, Baiker A. Flame aerosol synthesis of vanadia-titania nanoparticles: structural and catalytic properties in the selective catalytic reduction of NO by NH_3. J. Catal. 2001; 197:182–91.
53. Kammler HK, Pratsinis SE. Carbon-coated titania nanostructured particles: continuous, one-step flame-synthesis. J. Mater. Res. 2003; 18:2670–76.
54. Waser O, Büchel R, Hintennach A, Novák P, Pratsinis SE. Continuous flame aerosol synthesis of carbon-coated nano-$LiFePO_4$ for Li-ion batteries. J. Aerosol Sci. 2011; 42:657–67. [PubMed: 23407817]
55. Egerton TA. The modification of fine powders by inorganic coatings. KONA. 1998; 16:46–59.
56. Teleki A, Heine MC, Krumeich F, Akhtar MK, Pratsinis SE. In-situ coating of flame-made TiO_2 particles by nanothin SiO_2 films. Langmuir. 2008; 24:12553–58. [PubMed: 18850688]
57. Nienow AM, Roberts JT. Chemical vapor deposition of zirconium oxide on aerosolized silicon nanoparticles. Chem. Mater. 2006; 18:5571–77.
58. Buesser B, Pratsinis SE. Design of gas-phase synthesis of core-shell particles by computational fluid---aerosol dynamics. AIChE J. 2011; 57:3132–42.
59. Teleki A, Bjelobrk N, Pratsinis SE. Continuous surface functionalization of flame-made TiO_2 nanoparticles. Langmuir. 2010; 26:5815–22. [PubMed: 20192157]
60. King DM, Spencer JA Ii, Liang X, Hakim LF, Weimer AW. Atomic layer deposition on particles using a fluidized bed reactor with in situ mass spectrometry. Surf. Coat. Technol. 2007; 201:9163–71.
61. Liang X, Yu M, Li J, Jiang Y-B, Weimer AW. Ultra-thin microporous-mesoporous metal oxide films prepared by molecular layer deposition (MLD). Chem. Commun. 2009; 2009:7140–42.
62. Zhu WH, Pratsinis SE. Flame synthesis of nanosize powders---effect of flame configuration and oxidant composition. Nanotechnology. 1996; 622:64–78.
63. Walker KL, Geyling FT, Nagel SR. Thermophoretic deposition of small particles in the modified chemical vapor deposition (MCVD) process. J. Am. Ceram. Soc. 1980; 63:552–58.
64. Tsantilis S, Pratsinis SE. Soft- and hard-agglomerate aerosols made at high temperatures. Langmuir. 2004; 20:5933–39. [PubMed: 16459612]
65. Teleki A, Wengeler R, Wengeler L, Nirschl H, Pratsinis SE. Distinguishing between aggregates and agglomerates of flame-made TiO_2 by high-pressure dispersion. Powder Technol. 2008; 181:292–300.
66. Tricoli A, Graf M, Pratsinis SE. Optimal doping for enhanced SnO_2 sensitivity and thermal stability. Adv. Funct. Mater. 2008; 18:1969–76.
67. Keskinen H, Tricoli A, Marjamäki M, Mäkelä JM, Pratsinis SE. Size-selected agglomerates of SnO_2 nanoparticles as gas sensors. J. Appl. Phys. 2009; 106:084316.
68. Friedlander, SK. Smoke, Dust and Haze: Fundamentals of Aerosol Dynamics. Oxford Univ. Press; New York: 2000.
69. Jullien R, Kolb M, Botet R. Aggregation by kinetic clustering of clusters in dimensions d > 2. J. Phys. Lett. 1984; 45:211–16.
70. Meakin P, Jullien R. The effects of restructuring on the geometry of clusters formed by diffusion-limited, ballistic, and reaction-limited cluster-cluster aggregation. J. Chem. Phys. 1988; 89:246–50.
71. Eggersdorfer ML, Pratsinis SE. The structure of agglomerates consisting of polydisperse particles. Aerosol Sci. Technol. 2011; 46:347–53.
72. Akhtar MK, Lipscomb GG, Pratsinis SE. Monte Carlo simulation of particle coagulation and sintering. Aerosol Sci. Technol. 1994; 21:83–93.
73. Camenzind A, Schulz H, Teleki A, Beaucage G, Narayanan T, Pratsinis SE. Nanostructure evolution: from aggregated to spherical SiO_2 particles made in diffusion flames. Eur. J. Inorg. Chem. 2008; 2008:911–18.
73a. Eggersdorfer ML, Kadau D, Herrmann HJ, Pratsinis SE. Aggregate morphology evolution by sintering: number and diameter of primary particles. J. Aerosol Sci. 2012 In press.

74. Tsantilis S, Kammler HK, Pratsinis SE. Population balance modeling of flame synthesis of titania nanoparticles. Chem. Eng. Sci. 2002; 57:2139–56.
75. Xing HS, Koylu UO, Rosner DE. In situ light-scattering measurements of morphologically evolving flame-synthesized oxide nanoaggregates. Appl. Opt. 1999; 38:2686–97. [PubMed: 18319842]
76. Hyeon-Lee J, Beaucage G, Pratsinis SE, Vemury S. Fractal analysis of flame-synthesized nanostructured silica and titania powders using small-angle X-ray scattering. Langmuir. 1998; 14:5751–56.
77. Camenzind A, Schweizer T, Sztucki M, Pratsinis SE. Structure and strength of silica-PDMS nanocomposites. Polymer. 2010; 51:1796–804.
78. Park K, Cao F, Kittelson DB, McMurry PH. Relationship between particle mass and mobility for diesel exhaust particles. Environ. Sci. Technol. 2003; 37:577–83. [PubMed: 12630475]
79. Akhtar MK, Pratsinis SE, Mastrangelo SVR. Dopants in vapor-phase synthesis of titania powders. J. Am. Ceram. Soc. 1992; 75:3408–16.
80. Hinds, WC. Aerosol Technology: Properties, Behavior, and Measurement of Airborne Particles. Wiley; New York: 1999.
81. Strobel R, Pratsinis SE. Direct synthesis of maghemite, magnetite and wustite nanoparticles by flame spray pyrolysis. Adv. Powder Technol. 2009; 20:190–94.
82. Shannon RD, Pask JA. Topotaxy in the anatase-rutile transformation. Am. Mineral. 1964; 49:1707–17.
83. Seinfeld, JH.; Pandis, SN. Atmospheric Chemistry and Physics: From Air Pollution to Climate Change. Wiley; Hoboken, NJ: 2006. p. 1203
84. Eggersdorfer ML, Kadau D, Herrmann HJ, Pratsinis SE. Fragmentation and restructuring of soft-agglomerates under shear. J. Colloid Interf. Sci. 2010; 342:261–68.
85. Buesser B, Heine MC, Pratsinis SE. Coagulation of highly concentrated aerosols. J. Aerosol Sci. 2009; 40:89–100.
86. Matsui M, Akaogi M. Molecular dynamics simulation of the strucutral and physical properties of the four polymorphs of TiO_2. Mol. Simul. 1991; 6:239–44.
87. Buesser B, Gröhn AJ, Pratsinis SE. Sintering rate and mechanism of TiO_2 nanoparticles by molecular dynamics. J. Phys. Chem. C. 2011; 115:11030–35.
88. Thompson SM, Gubbins KE, Walton JPRB, Chantry RAR, Rowlinson JS. A molecular dynamics study of liquid drops. J. Chem. Phys. 1984; 81:530–42.
89. Hamad S, Catlow CRA, Woodley SM, Lago S, Mejías JA. Structure and stability of small TiO_2 nanoparticles. J. Phys. Chem. B. 2005; 109:15741–48. [PubMed: 16852997]
90. Rosner, DE. Transport Processes in Chemically Reacting Flow Systems. Butterworths; Stoneham, MA: 1986.
91. Gelbard F, Seinfeld JH. Simulation of multicomponent aerosol dynamics. J. Colloid Interf. Sci. 1980; 78:485–501.
92. Xiong Y, Pratsinis SE. Formation of agglomerate particles by coagulation and sintering. Part I. A two-dimensional solution of the population balance equation. J. Aerosol Sci. 1993; 24:283–300.
93. Xiong Y, Akhtar MK, Pratsinis SE. Formation of agglomerate particles by coagulation and sintering. Part II. The evolution of the morphology of aerosol-made titania, silica and silica-doped titania powders. J. Aerosol Sci. 1993; 24:301–13.
94. Kruis FE, Kusters KA, Pratsinis SE, Scarlett B. A simple model for the evolution of the characteristics of aggregate particles undergoing coagulation and sintering. Aerosol Sci. Technol. 1993; 19:514–26. [Describes the simplest aerosol particle dynamics; it captures all relevant mechanisms that are based on omnipresent aerosol properties.]
95. Poon JMH, Immanuel CD, Doyle FJ III, Litster JD. A three-dimensional population balance model of granulation with a mechanistic representation of the nucleation and aggregation phenomena. Chem. Eng. Sci. 2008; 63:1315–29.
96. Lee KW. Change of particle size distribution during Brownian coagulation. J. Colloid Interf. Sci. 1983; 92:315–25.

97. Whitby ER, McMurry PH. Modal aerosol dynamics modeling. Aerosol Sci. Technol. 1997; 27:673–88.
98. Frenklach M. Method of moments with interpolative closure. Chem. Eng. Sci. 2002; 57:2229–39.
99. McGraw R. Description of aerosol dynamics by the quadrature method of moments. Aerosol Sci. Technol. 1997; 27:255–65.
100. Rosner DE, McGraw R, Tandon P. Multivariate population balances via moment and Monte Carlo simulation methods: an important sol reaction engineering bivariate example and “mixed” moments for the estimation of deposition, scavenging, and optical properties for populations of nonspherical suspended particles. Ind. Eng. Chem. Res. 2003; 42:2699–711.
101. Marchisio DL, Fox RO. Solution of population balance equations using the direct quadrature method of moments. J. Aerosol Sci. 2005; 36:43–73.
102. Kim K-S, Pratsinis SE. Modeling and analysis of modified chemical vapor deposition of optical fiber preforms. Chem. Eng. Sci. 1989; 44:2475–82.
103. Friedlander SK, Wang CS. The self-preserving particle size distribution for coagulation by brownian motion. J. Colloid Interface Sci. 1966; 22:126–32.
104. Heine MC, Pratsinis SE. Brownian coagulation at high concentration. Langmuir. 2007; 23:9882–90. [PubMed: 17685639]
105. Landgrebe JD, Pratsinis SE. Gas-phase manufacture of particulates: interplay of chemical reaction and aerosol coagulation in the free-molecular regime. Ind. Eng. Chem. Res. 1989; 28:1474–81.
106. Mitchell P, Frenklach M. Particle aggregation with simultaneous surface growth. Phys. Rev. E. 2003; 67:061407.
107. Vemury S, Pratsinis SE. Self-preserving size distributions of agglomerates. J. Aerosol Sci. 1995; 26:175–85.
108. Koch W, Friedlander SK. The effect of particle coalescence on the surface area of a coagulating aerosol. J. Colloid Interface Sci. 1990; 140:419–27. [A widely used phenomenological model for the surface area evolution during sintering of aerosol particles.]
109. Kirchhof MJ, Schmid HJ, Peukert W. Three-dimensional simulation of viscous-flow agglomerate sintering. Phys. Rev. E. 2009; 80:026319.
110. Heine MC, Pratsinis SE. Polydispersity of primary particles in agglomerates made by coagulation and sintering. J. Aerosol Sci. 2007; 38:17–38.
111. Ulrich GD. Theory of particle formation and growth in oxide synthesis flames. Combust. Sci. Technol. 1971; 4:47–57.
112. Xiong Y, Pratsinis SE. Gas-phase production of particles in reactive turbulent flows. J. Aerosol Sci. 1991; 22:637–55.
113. Warren DR, Seinfeld JH. Nucleation and growth of aerosol from a continuously reinforced vapor. Aerosol Sci. Technol. 1984; 3:135–53.
114. Jeong JI, Choi M. A simple bimodal model for the evolution of non-spherical particles undergoing nucleation, coagulation and coalescence. J. Aerosol Sci. 2003; 34:965–76.
115. Pratsinis SE, Bai H, Biswas P, Frenklach M, Mastrangelo SVR. Kinetics of titanium(IV) chloride oxidation. J. Am. Ceram. Soc. 1990; 73:2158–62.
116. Powers DR. Kinetics of $SiCl_4$ oxidation. J. Am. Ceram. Soc. 1978; 61:295–97.
117. Gröhn AJ, Buesser B, Jokiniemi JK, Pratsinis SE. Design of turbulent flame aerosol reactors by mixing-limited fluid dynamics. Ind. Eng. Chem. Res. 2011; 50:3159–68.
118. Yu S, Yoon Y, Müller-Roosen M, Kennedy IM. A two-dimensional discrete-sectional model for metal aerosol dynamics in a flame. Aerosol Sci. Technol. 1998; 28:185–96.
119. Seto T, Hirota A, Fujimoto T, Shimada M, Okuyama K. Sintering of polydisperse nanometer-sized agglomerates. Aerosol Sci. Technol. 1997; 27:422–38.
120. Seto T, Shimada M, Okuyama K. Evaluation of sintering of nanometer-sized titania using aerosol method. Aerosol Sci. Technol. 1995; 23:183–200.
121. Swihart MT, Girshick SL. Thermochemistry and kinetics of silicon hydride cluster formation during thermal decomposition of silane. J. Phys. Chem. B. 1999; 103:64–76.

122. Dang H, Swihart MT. Computational modeling of silicon nanoparticle synthesis: II. A two-dimensional bivariate model for silicon nanoparticle synthesis in a laser-driven reactor including finite-rate coalescence. Aerosol Sci. Technol. 2009; 43:554–69.
123. Körmer R, Schmid HJ, Peukert W. Aerosol synthesis of silicon nanoparticles with narrow size distribution. Part 2: Theoretical analysis of the formation mechanism. J. Aerosol Sci. 2010; 41:1008–19.
124. Hannebauer B, Menzel F. The combustion of $SiCl_4$ in hot O_2/H_2 flames. Z. Anorg. Allg. Chem. 2003; 629:1485–90.
125. West RH, Shirley RA, Kraft M, Goldsmith CF, Green WH. A detailed kinetic model for combustion synthesis of titania from $TiCl_4$. Combust. Flame. 2009; 156:1764–70.
126. Skillas G, Becker C, Mühlenweg H, Behnisch J. Simulation of particulates in a carbon black reactor. J. Nanopart. Res. 2005; 7:15–27.
127. Heine MC, Pratsinis SE. High concentration agglomerate dynamics at high temperatures. Langmuir. 2006; 22:10238–45. [PubMed: 17107027]
128. Bromley ST, Illas F. Energetics and structures of the initial stages of nucleation of (SiO_2) species: possible routes to highly symmetrical tetrahedral clusters. Phys. Chem. Chem. Phys. 2007; 9:1078–86. [PubMed: 17311150]
129. Shirley R, Kraft M, Inderwildi OR. Electronic and optical properties of aluminium-doped anatase and rutile TiO_2 from ab initio calculations. Phys. Rev. B. 2010; 81:075111.
130. Mezey, EJ. Pigments and reinforcing agents. In: Powell, CF.; Oxley, JH.; Blocher, JM., editors. Vapor Deposition. Wiley; New York: 1966. p. 423-51.
131. Bensberg A, Roth P, Brink R, Lange H. Modeling of particle evolution in aerosol reactors with coflowing gaseous reactants. AIChE J. 1999; 45:2097–107.
132. Shih T-H, Liou WW, Shabbir A, Yang Z, Zhu J. A new k-ε eddy viscosity model for high Reynolds number turbulent flows. Comput. Fluids. 1995; 24:227–38.
133. Launder BE, Reece GJ, Rodi W. Progress in the development of a Reynolds-stress turbulence closure. J. Fluid. Mech. 1975; 68:537–66.
134. Hoekstra AJ, Derksen JJ, Van Den Akker HEA. An experimental and numerical study of turbulent swirling flow in gas cyclones. Chem. Eng. Sci. 1999; 54:2055–65.
135. Johannessen T, Pratsinis SE, Livbjerg H. Computational analysis of coagulation and coalescence in the flame synthesis of titania particles. Powder Technol. 2001; 118:242–50.
136. Ji Y, Sohn HY, Jang HD, Wan B, Ring TA. Computational fluid dynamic modeling of a flame reaction process for silica nanopowder synthesis from tetraethylorthosilicate. J. Am. Ceram. Soc. 2007; 90:3838–45.
137. Jang HD. Experimental study of synthesis of silica nanoparticles by a bench-scale diffusion flame reactor. Powder Technol. 2001; 119:102–8.
138. Manenti G, Masi M. Numerical investigation on new configurations for vapor-phase aerosol reactors. Chem. Eng. Sci. 2009; 64:3525–35.
139. Settumba N, Garrick SC. Direct numerical simulation of nanoparticle coagulation in a temporal mixing layer via a moment method. J. Aerosol Sci. 2003; 34:149–67.
140. Yu M, Lin J, Chen L. Nanoparticle coagulation in a planar jet via moment method. Appl. Math. Mech. 2007; 28:1445–53.
141. Mehta M, Sung Y, Raman V, Fox RO. Multiscale modeling of TiO_2 nanoparticle production in flame reactors: Effect of chemical mechanism. Ind. Eng. Chem. Res. 2010; 49:10663–73.
142. Sung Y, Raman V, Fox RO. Large-eddy-simulation-based multiscale modeling of TiO_2 nanoparticle synthesis in a turbulent flame reactor using detailed nucleation chemistry. Chem. Eng. Sci. 2011; 66:4370–81.
143. Pratsinis SE, Zhu W, Vemury S. The role of gas mixing in flame synthesis of titania powders. Powder Technol. 1996; 86:87–93.
144. Ostraat M, De Blauwe J, Green M, Bell L, Brongersma M, et al. Synthesis and characterization of aerosol silicon nanocrystal nonvolatile floating-gate memory devices. Appl. Phys. Lett. 2001; 79:433.

145. Patey TJ, Büchel R, Ng SH, Krumeich F, Pratsinis SE, Novák P. Flame co-synthesis of $LiMn_2O_4$ and carbon nanocomposites for high power batteries. J. Power Sources. 2009; 189:149–54.

146. Righettoni M, Tricoli A, Pratsinis SE. Si:WO_3 sensors for highly selective detection of acetone for easy diagnosis of diabetes by breath analysis. Anal. Chem. 2010; 82:3581–87. [PubMed: 20380475]

147. Madler L, Stark WJ, Pratsinis SE. Rapid synthesis of stable ZnO quantum dots. J. Appl. Phys. 2002; 92:6537–40.

148. Brunner TJ, Wick P, Manser P, Spohn P, Grass RN, et al. In vitro cytotoxicity of oxide nanoparticles: comparison to asbestos, silica, and the effect of particle solubility. Environ. Sci. Technol. 2006; 40:4374–81. [PubMed: 16903273] [Early detailed comparison of the cytotoxicity of nanoparticles composed of various materials that was proposed as screening method.]

149. Demou E, Stark WJ, Hellweg S. Particle emission and exposure during nanoparticle synthesis in research laboratories. Ann. Occup. Hyg. 2009; 53:829–38. [PubMed: 19703918]

150. Demokritou P, Büchel R, Molina RM, Deloid GM, Brain JD, Pratsinis SE. Development and characterization of a versatile engineered nanomaterial generation system (VENGES) suitable for toxicological studies. Inhal. Toxicol. 2010; 22:107–16. [PubMed: 20701428] [A review of an array of products made by aerosol technology.]

151. Deleted in proof

RELATED RESOURCES

Seinfeld JH, Pankow JF. Organic atmospheric particulate material. Annu. Rev. Phys. Chem. 2003; 54:121–40. [PubMed: 12524426]

Baiker A, Mallat T. Potential of supported gold nanoparticles for the synthesis of fine chemicals. Annu. Rev. Chem. Biomol. Eng. 2012; 3 In press.

Xia T, Li N, Nel AE. Potential health impact of nanoparticles. Annu. Rev. Publ. Health. 2009; 30:137–50.

Wang AZ, Langer RS, Farokhzad OC. Nanoparticle delivery of cancer drugs. Annu. Rev. Med. 2012; 63 In press.

Beveridge JS, Stephens JR, Williams ME. The use of magnetic nanoparticles in analytical chemistry. Annu. Rev. Anal. Chem. 2011; 4:251–73.

Swihart MT. Vapor-phase synthesis of nanoparticles. Curr. Opin. Colloid Interface Sci. 2003; 8:127–33.

Roth P. Particle synthesis in flames. Proc. Combust. Inst. 2007; 31:1773–88.

Biskos G, Vons V, Yuteri CU, Scmidt-Ott A. Generation and sizing of aerosol-based nanotechnology. Kona Powder Part. J. 2008; 26:13–35.

Mezey, EJ. Pigments and reinforcing agents. In: Palmer, CF.; Oxley, JH.; Blocher, JM., editors. Vapor Deposition. John Wiley & Sons; New York, NY: 1966. p. 423-51.

Cabot, TD. Beggar on Horseback. Godine; Boston, MA: 1979.

Europe PMC Funders Author Manuscripts

Europe PMC Funders Author Manuscripts

SUMMARY POINTS

1. Aerosol processes are advantageous for scalable synthesis of nanomaterials because they offer no liquid by-products, easy particle collection, few process steps, and rigorous transport phenomena (e.g., diffusion), features that facilitate process design that leads to high-purity products (e.g., optical fibers), unique filamentary morphology, and nonequilibrium, metastable phases.
2. Aerosol processes are used to make carbon blacks, most pigmentary TiO_2, fumed silica (and other oxides) for pharmaceuticals, optical fibers and microelectronics, filamentary metals, and ceramic films and powders.
3. Flame reactors dominate the value and volume of aerosol-made materials.
4. The presence of high particle concentrations in aerosol manufacturing leads to rapid attainment of the SPSD by Brownian coagulation. This simplifies the description of particle dynamics by monitoring a single moment of their distribution (e.g., number).
5. Fractal theory describes well the ramified structure of aerosol-made materials.
6. Sintering narrows the size distribution of the constituent PPs in aggregates.
7. The ratio of characteristic coagulation to sintering time during aerosol formation and growth determines the extent of particle aggregation.
8. Aerosol-made materials contribute to the development of novel catalysts, gas sensors, biomaterials, electroceramics, and even nutritional materials.

Europe PMC Funders Author Manuscripts

FUTURE ISSUES

1. Development of more efficient descriptions of chemistry, fluid flow, and particle dynamics during aerosol synthesis of materials is needed to create predictive models for aerosol process design and operation.
2. Synthesis of nanoparticles of mixed composition or encapsulated with several layers or functional molecules requires more detailed, multiscale models accounting for the chemistry of material interactions to predict optimal reactor conditions.
3. Doping of nanoparticles with tracer concentrations of other elements changes physical and chemical properties dramatically, and future models will need to account for the influence of doping atom type, concentration, and location on sintering rate, crystal phase, surface reactivity, etc.
4. Quantifying the influence of doping atoms, surface molecules, and crystal composition on characteristic sintering rates will lead to a better understanding of the sintering of nanoparticles in the gas phase and eventually to optimal process design.
5. Incorporation of particles directly from the gas phase into devices and applications simplifies their manufacture while minimizing process steps.
6. Fractal-like particles exhibit specific rates for transport, coagulation, sintering, restructuring, and even fragmentation that are so far often approximated by models originally developed for spherical (nonfractal) particles. Future models will determine separate rates for mechanisms involving fractal-like particles as function of their size and fractality.
7. Development of further life science applications of nanoparticles for therapeutic, diagnostic, and drug delivery applications by designing and optimizing aerosol processes experimentally guided by modeling and simulation has a lot of potential.
8. Coagulation is the dominant process for nanoparticle growth, and its rate is quantified assuming that every collision leads to attaching particles. Sticking efficiencies of nanoparticles upon collision as a function of surface structures, such as texture, coating shells, and functional surface molecules will provide more exact coagulation rates.

Europe PMC Funders Author Manuscripts

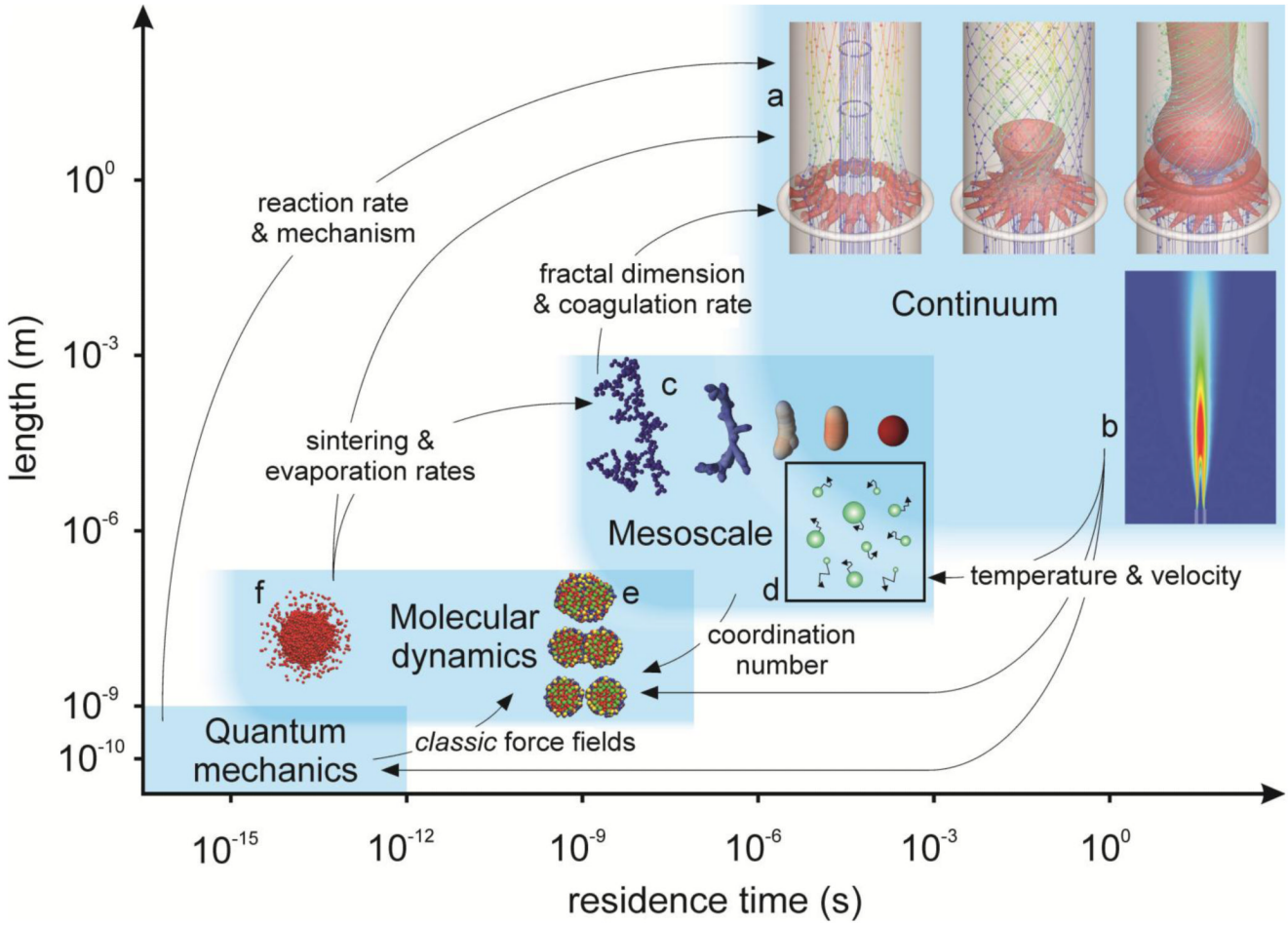

Figure 1.

Overview of the time and length scales for continuum, mesoscale, molecular dynamics (MD), and quantum mechanics models of the aerosol synthesis of materials. The upper boundary of each model is defined mostly by computational demands, whereas the lower boundary is fuzzier, and areas can overlap. The arrows between the models indicate exchange of information between them. Insets show representative model results of (*a*) the effect of mixing aerosol and precursor vapor on in-situ coating of flame-made TiO_2, Ag, or Fe_2O_3 nanoparticles by SiO_2 films (58); (*b*) SiO_2 particle formation in diffusion flames (117); (*c*) agglomerate evolution by sintering to aggregates and eventually to compact particles (84); (*d*) the coagulation of highly concentrated aerosols (85); (*e*) an MD model of TiO_2 nanoparticle sintering from surface to grain boundary diffusion and gradual attainment of bulk sintering rates at approximately 5 nm in diameter (87); and (*f*) an MD model of nanodroplet evaporation (90). Panel *a* reprinted and adapted with permission from *AIChE Journal*, copyright © 2011 AIChE. Panels *b*, c, and *e* reprinted and adapted with permission from *Industrial and Engineering Chemistry Research* (panel *b*), *Langmuir* (panel *c*), and *Journal of Physical Chemistry C* (panel *e*), copyright © 2011 American Chemical Society.

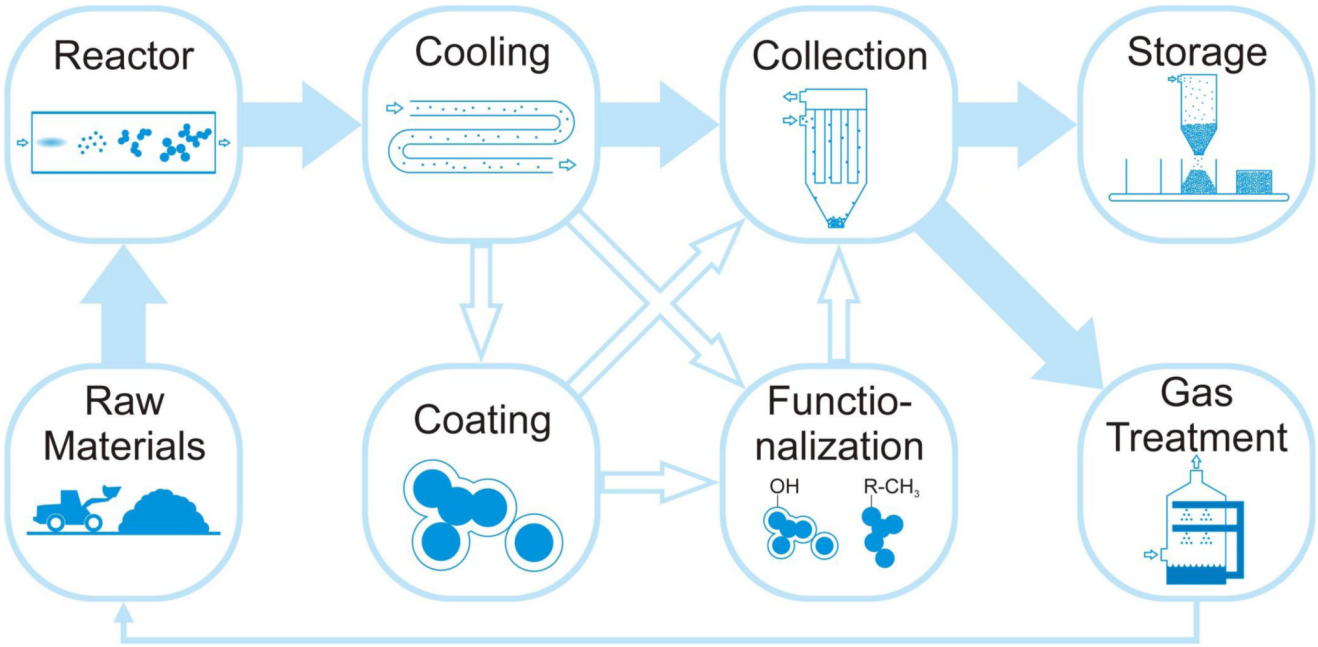

Figure 2.
The process cycle of aerosol manufacturing starts with the preparation of raw materials by mining and refining ores or by using recycled gases and liquid precursors. Reactors transform these raw materials into nanomaterials through aerosol processes driven by high temperatures, which are followed by cooling to stop nanoparticle growth. Depending on the desired product properties, particles are collected from the gas phase immediately or are conditioned by aerosol coating and/or functionalization steps. Particles are stored and packaged depending on customer needs, whereas the gases are cleaned and where possible recycled from the same process (e.g., chlorine for extraction of titanium from its ore) or sold as products.

Europe PMC Funders Author Manuscripts

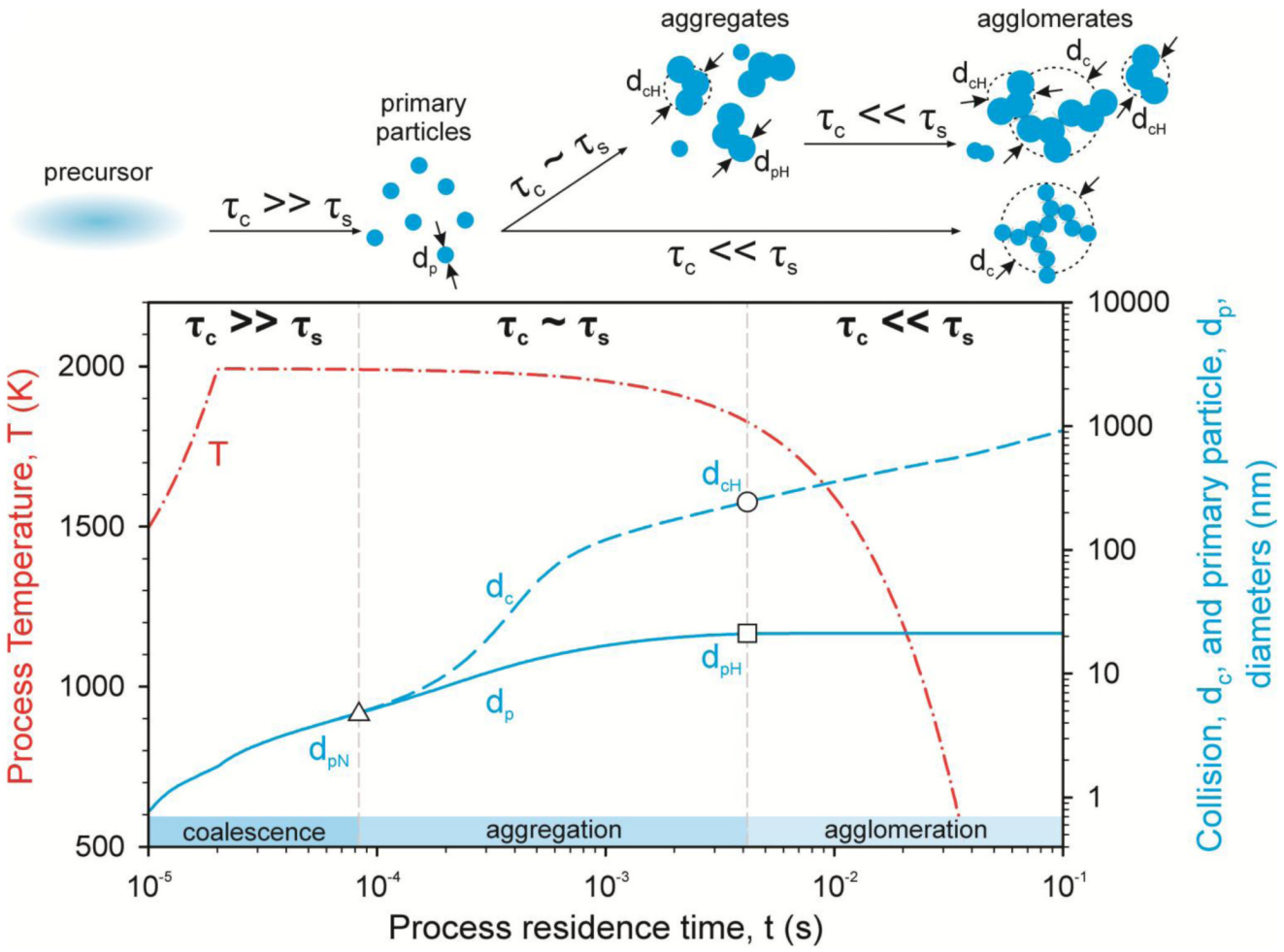

Figure 3.

Overview of aerosol growth by coagulation and sintering showing the evolution of primary particle (PP) diameter, d_p (*blue solid line*), and agglomerate collision diameter, d_c (*blue dashed line*), with a typical temperature profile (*red dash-dot line*) (127) along with the relative magnitude of the characteristic times of coagulation, τ_c, and sintering, τ_s. The evolution can be divided into three stages: full coalescence ($\tau_c >> \gamma_s$), aggregation ($\tau_c \sim \tau_s$), and agglomeration ($\tau_c << \tau_s$); the first and second stages determine the PP and average aggregate sizes, whereas the second and third stages determine the agglomerate size (64). The length of the middle stage ($\tau_c \sim \tau_s$) determines if agglomerates of aggregates (*top, upper path*) or of spherical particles (*top, lower path*) are formed---in other words, the extent of aggregate formation and hard bonding between PPs (d_{cH}/d_{pH}). For $d_{cH}/d_{pH} \rightarrow 1$, few, if any, aggregates are formed.